Investigation of precession laser machining of micro-holes in aerospace material

Le, Hoang; Nasrollahi, Vahid; Karkantonis, Themistoklis; Penchev, Pavel; Marimuthu, Sundar; Crozier, Mickey; Dimov, Stefan

DOI:
10.2351/7.0000903

Journal of Laser Applications

Investigation of precession laser machining of microholes in aerospace material

Cite as: J. Laser Appl. **35**, 012028 (2023); https://doi.org/10.2351/7.0000903
Submitted: 05 November 2022 • Accepted: 28 January 2023 • Published Online: 21 February 2023
Published open access through an agreement with JISC Collections

Hoang Le, Vahid Nasrollahi, Themistoklis Karkantonis, et al.

Journal of Laser Applications ARTICLE scitation.org/journal/jla

Investigation of precession laser machining of microholes in aerospace material

Cite as: J. Laser Appl. 35, 012028 (2023); doi: 10.2351/7.0000903
Submitted: 5 November 2022 · Accepted: 28 January 2023 ·
Published Online: 21 February 2023

Hoang Le,[1,a)] Vahid Nasrollahi,[1] Themistoklis Karkantonis,[1] Pavel Penchev,[1] Sundar Marimuthu,[2] Mickey Crozier,[2] and Stefan Dimov[1]

AFFILIATIONS

[1]Department of Mechanical Engineering, University of Birmingham, Birmingham B15 2TT, United Kingdom
[2]The Manufacturing Technology Centre Ltd, Coventry CV7 9JU, United Kingdom

[a)]**Author to whom correspondence should be addressed; electronic mail:** hxl683@student.bham.ac.uk

ABSTRACT

Sidewall tapering is one of the main limitations in ultrashort pulse (USP) laser machining and is associated with the beam shape and self-limiting effect. Laser processing with a precession beam is a potential solution to overcome this limitation. A study into the effects of precession parameters on the taper angle in microhole drilling of a nickel alloy is reported in this paper. The effects of three key precession parameters, i.e., incident angle, relative distance between the focuses of the precession and individual beams, and scanning speed, have been investigated in detail. Experiments were performed to drill through holes with aspect ratios up to 20:1 and diameters ranging from 100 to 500 μm over 0.6–2 mm thick nickel alloy substrates. Experiment results showed that all the considered parameters/factors were significant and affected the hole tapering in different ways. In addition, there were important interaction effects between two of the factors, i.e., incident angle and focus position, in some cases. The optimal parameters to minimize the tapering effect are suggested, and the mechanism is discussed in detail. The precession laser machining showed clear advantages in overcoming the limitations to associated with conventional USP laser machining. Fabricating microholes with high geometrical accuracy, i.e., with straight side walls and zero taper angles, is feasible with the use of a precession beam. The results clearly show the potential of precession laser processing and the capabilities that the technology can offer for a range of laser micromachining applications in different industries, such as microelectronics, automotive, and aerospace.

Key words: precession, ultrashort pulse laser, microhole, optimization, nickel alloys.

I. INTRODUCTION

The use of laser micromachining technology for hole drilling has widely been known in manufacturing industry, especially when quality and accuracy are the main requirements.[1] Typical applications of laser microdrilling can be found in numerous fields such as microfluidic, biomedical, and microelectronic devices or automotive and aerospace components.[2–5] Generally, key technical requirements in laser microdrilling are the hole's aspect ratio, geometrical and dimensional accuracy, and the overall process efficiency. Also, the quality of laser-drilled microholes can be impacted by the heat-affected zone and redepositions of material that typically appear at the entrance of the holes.[6] At the same time, the process efficiency is mainly assessed by either the material removal rate or machining time. Due to constant advancements in laser technology and beam delivery subsystems, different approaches/methods have been developed and deployed to improve the laser microdrilling process. Specifically, there are two main approaches to improve the laser micromachining process, i.e., through changes of laser beam properties (e.g., energy, shape, and pulse duration) or relative movements between the laser beam and the workpiece. In the case of pulsed lasers, microdrilling can be performed with various pulse durations, from ultrashort to short or long pulse widths. Short and long laser pulses with widths from subnanosecond to millisecond usually used for achieving high removal rates at the expense of machining quality,[7,8] like thermal damage. On the contrary, USP lasers are preferred when high-quality holes are required because the ablation mechanism is almost athermal and the heat-affected zone would be minimal.[9,10]

Changing the beam spatial profile through beam shaping is also a potential solution for minimizing any negative tapering effects in microholes that are laser drilled.[11] Apart from the Gaussian beam profile that is widely used, a top-hat (or flat-top) beam is used for improving the processing quality and efficiency, i.e., for reducing the taper angles and increasing material removal rates.[12] In addition, it should be noted that beam polarization, pulse repetition rates, and fluence levels are also process variables that affect laser microdrilling operations.[13]

The second approach widely used to improve the microdrilling process is through the introduction of a beam motion and, thus, to achieve more efficient and precise ablation. Specifically, relative movements between the beam and the workpiece are employed in laser microdrilling that are usually implemented through scanning strategies and by varying the incident/attacking angle of the laser beam. Typical scanning strategies used for laser microdrilling operations are single-pulse drilling, hatching, percussion, helical drilling, and trepanning.[6,14–16] Single-pulse drilling and percussion drilling are generally employed when a hole diameter equal to the beam spot size is required, whereas the other strategies are applied for hole diameters larger than the beam spot size. The helical drilling and trepanning strategies are used to distribute laser energy evenly along the hole contour and, thus, to ablate material only in those areas rather than to ablate all materials within the holes as it is the case in hatching ones. As a result, these drilling strategies can reduce the taper angle with the increase in the hole depth and can minimize the machining time. Despite the different scanning strategies were studied and applied on USP laser micromachining, these solution still cannot eliminate completely the tapering effect in laser microdrilling or micromilling and, thus, to enable the manufacture of vertical wall due to the inherent properties of Gaussian laser beams.[17,18]

The tapering effect is mostly attributed to the increase in the size of the laser-material interaction zone, at the side wall, and the self-limiting effect leading to the drop of fluence levels and low ablation efficiency, consequently.[19,20] Therefore, a rational solution to overcome this issue is to increase the ablation efficiency, i.e., the laser fluence, at the side walls of microholes. However, to achieve this, the laser beam should not be normal to the substrate surface anymore and instead should be approaching at a given incident angle; for example, the beam can perform relative precession movements in regard to the workpiece.[21] Such precession movements can be performed by either the workpiece or the beam. The latter is preferable because it can offer a higher flexibility and can be executed more efficiently. Currently, there are commercial laser systems on the market that offer such capabilities, i.e., beam precession movements for improving microdrilling and cutting processes.[22–26] There are some common key parameters in such precession processing systems, such as incident angle and linear and rotary speed of the precession beam together with its focusing position. However, the role and significance of these parameters and their interactions in precession microdrilling have not been investigated systematically, and thus, there is a significant knowledge gap in this topic.

Therefore, this study investigates the underlying mechanism of precession laser processing with the objective to understand the laser microdrilling process in more details. The influence of key precession parameters is investigated systematically, and their effects on the laser microdrilling process are analyzed. A popular aerospace alloy, i.e., nickel-based super alloy C263, has been selected to carry out this empirical research, and thus, the results are of a specific interest to aerospace applications of the microdrilling process. However, C263 is an alloy and has similar mechanism with other metal-based materials in laser ablation; therefore, the conclusions made could be considered more generic, especially about the precession microdrilling capabilities, and can inform other potential applications of this technology.[27–29]

II. METHODOLOGY AND MATERIALS

A. Laser micromachining system

The research reported in this study was carried out on a LASEA LS-4 laser processing workstation that integrates a diode-pumped pulsed laser source with a pulse duration of approximately 500 fs at the central wavelength of 1030 nm. The athermal ablation mechanism of this USP laser source allows laser processing with almost negligible negative side effects, and therefore, the effects of different parameters on quality of produced microstructures can be seen clearer. The same pulse energy at the workpiece, i.e., 60 μJ at a frequency of 100 kHz, was used in all experiments. The laser pulse energy was controlled based on the applied frequency and laser power after the focusing lens measured by a power meter. The beam had circular polarization and was focused through a telecentric lens with a focal distance of 100 mm onto a spot size of 30 μm (measured by a camera-based beam profiler) and the peak fluence was 16.98 J/cm^2 at the focal plane. A simplified diagram of the laser processing workstation is provided in Fig. 1.

The precession movements of the laser beam after focusing lens are produced by a module, called LS-Precess, which is integrated into the beam delivery subsystem between the beam conditioning module and the XY scan head. The precession laser machining principals are described in detail in Refs. 30 and 31. The rotary speed of the precession beam after focusing lens can be varied from 0 to 3141 rad/s. However, only the maximum rotary

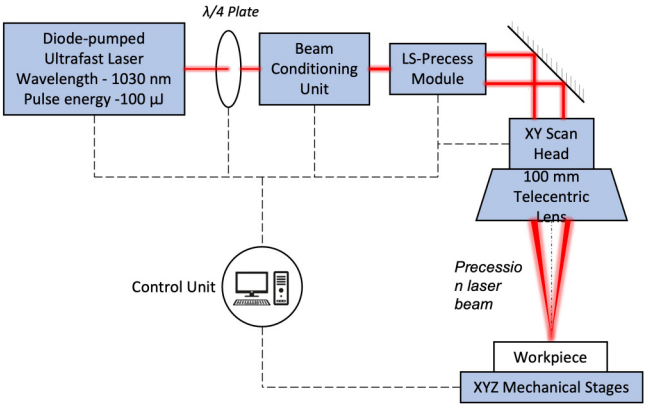

FIG. 1. Diagram of the laser processing workstation with its key components.

speed was used in this experimental study to achieve the highest possible machining efficiency on this laser processing workstation.

The two important precession parameters investigated in this research are illustrated in Fig. 2. The first key parameter is the incident angle of the laser beam, which is defined by the angle between the beam and the central axis of the focusing lens. The incident angle can be varied on the LS4-workstation in the range from 2.86° to 4.27° by changing the diameter of the precession beam before focusing lens with the LS-Precess module, as shown in Figs. 2(a) and 2(b).[30] However, there was a clipping of the precession beam at the entrance of the scan head when the incident angle was greater than 3.56°. Thus, to avoid the significant drop of the laser power and the deterioration of beam quality after focusing lens, the incident angle was varied from 2.86° to 3.56° only. The interdependence between the incident angle and the diameter of the precession beam is depicted in Fig. 3. This functional dependence can potentially affect the drilling process when relatively thick substrates are machined using bigger incident angles while

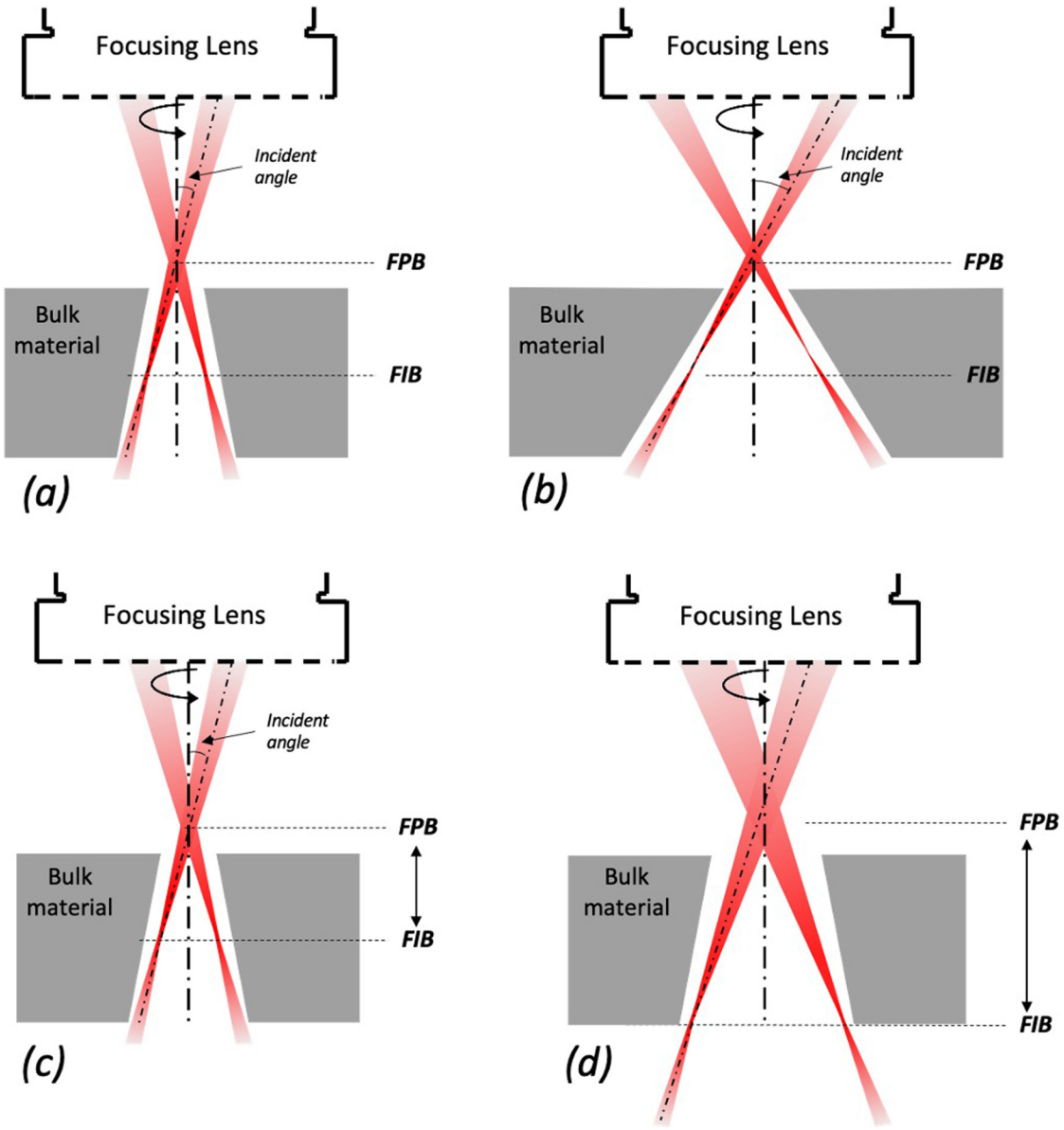

FIG. 2. An illustration of the precession laser beam in interaction with the material while varying key processing parameters: (a) small incident angle; (b) large incident angle; (c) small FPB-FIB distance; and (d) large FPB-FIB distance. Note: FPB refers to the focus of the precession beam, while FIB is the focus of the individual beam.

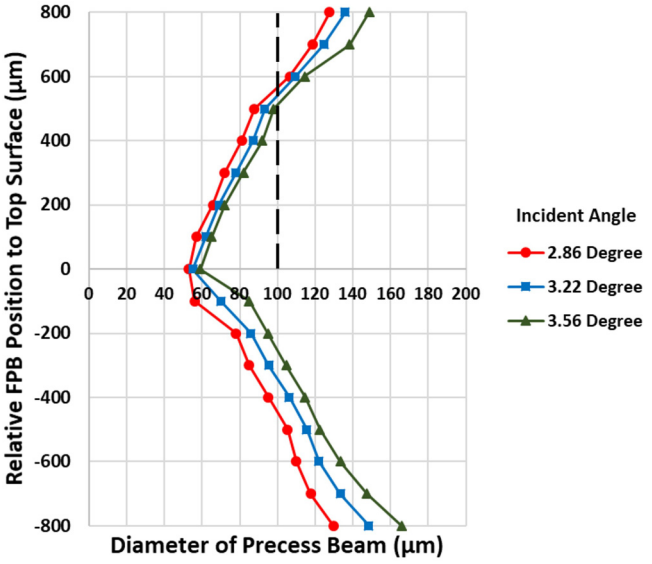

FIG. 3. Measured diameters of the precession beam with three different incident angles at different positions along the focusing lens axis. Precession beam diameters were measured experimentally by machining straight lines on a silicon wafer with a single pass at different FPB positions. The beam diameter is determined by the width of machined lines.

the precession beam is translated downward. Consequently, the beam could be partially blocked by the structure edge, and therefore, the design of an appropriate machining strategy is essential for a successful microdrilling operation.

The second key parameter investigated in this study is the distance between the focus of the precession beam (FPB) and the focus of the individual beam (FIB) [Figs. 2(c) and 2(d)]. FPB is the point along the focusing lens axis where the precession beam has the smallest diameter, while FIB is the beam focus where the laser fluence reaches the highest value. Therefore, the FPB-FIB distance plays an important role in achieving the required dimensional accuracy together with a higher ablation efficiency. It is possible to vary the FPB-FIB distance from 400 to 900 μm, approximately, on the LS4 workstation, and its variation does not affect the precession beam diameter. However, a reduction in laser power was observed when the FPB-FIB distance had been increasing.

The third key parameter investigated in this research was the linear scanning speed of the precession beam. The precession beam path is a combination of its circular and linear scanning motion that leads to a spiral trajectory. As the beam rotational speed is usually kept at its maximum value, the scanning speed is an essential factor for controlling the overlap level between laser pulses. Thus, the resulting trepanning strategy allows the removal rate together with the edge definition of microstructures[32] to be controlled. The effects of scanning speed on the beam path and the pulse overlap level is depicted in Fig. 4.

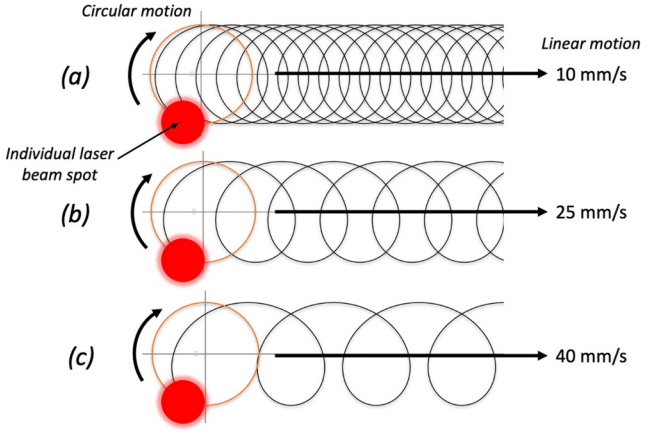

FIG. 4. Laser beam paths with different scanning speeds and rotational speed of 3141 rad/s when FIB is at the top surface of the workpiece: (a) 10, (b) 25, and (c) 40 mm/s.

B. Materials

The precession laser microdrilling was investigated and optimized for a nickel-based super alloy, i.e., C263, that is well known for its high strength and excellent resistance to oxidation under extreme working conditions.[33,34] These properties make C263 an ideal material for producing different components for turbine applications, e.g., in aerospace and powerplants.[35] Laser microdrilling is a desirable solution to manufacture feature, such as cooling holes on turbine blades. Specifically, the high precision and accuracy that can be achieved with precession laser processing can offer performance and quality improvements of such functional features for turbine applications. Nickel-based super alloy C263 plate with thicknesses from 0.6 to 2 mm was used in the experiments of this research.

C. Design of experiment (DoE)

1. Machining strategies

The precession drilling strategies were investigated on the machining of holes with three diameters, i.e., 100, 250, and 500 μm, on C263 plates with three thicknesses, 0.6, 1, and 2 mm. Different precession drilling strategies were required to produce those holes on the samples due to differences in their diameters and sample thickness (or holes' aspect ratio). Therefore, initial trials were conducted to identify suitable strategies and define the parameter range for this research.

The precession drilling strategies for different hole diameters and substrate thicknesses were designed to be as simple as possible for execution and the differences between them to be minimal in order to minimize their influence on the machining results. Therefore, a family of outlining strategies was employed to machine the holes with different diameters as depicted in Fig. 5. The laser beam spot size was taken into account in adjusting the outlining diameters with the objective to machine holes as close as possible to target dimensions. In general, the thicker samples required a

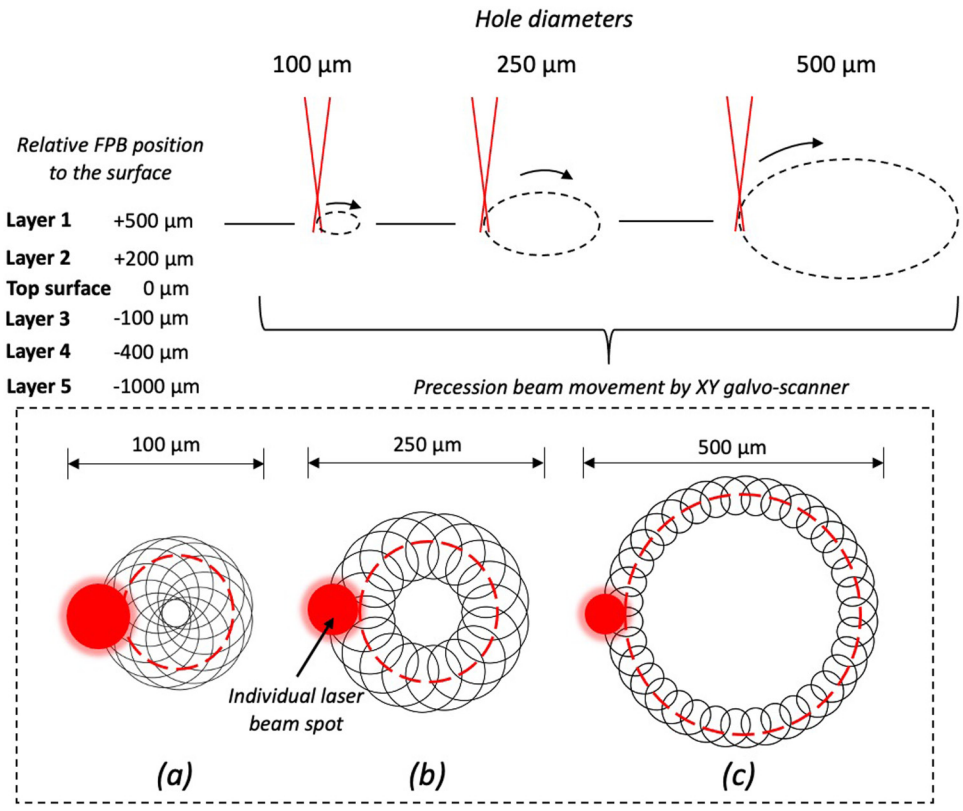

FIG. 5. Top: the family of precession strategies used to drill microholes with different diameters in the plates with three thicknesses. Bottom: an example of the paths of the individual beam (black line) at maximum rotational speed of 3141 rad/s and the precession beam (red dashed line) at linear scanning speed of 40 mm/s when drilling holes with different diameters: (a) 100 μm, (b) 250 μm, and (c) 500 μm. Note: The beam spot sizes in (a)–(c) are the same for different diameters in reality. The difference in spot size in figure is for illustration purpose.

high number of FPB adjustments, referred to layers of outlining passes in this research, to refocus the precession laser beam and, thus, to maintain an efficient laser ablation at a higher hole depth. Specifically, as it was already stated, plates with three thicknesses were used, i.e., 0.6, 1, and 2 mm, and their holes were produced with one layer (layer 1), three layers (layers 1–3), and five layers (layers 1–5), respectively. The number of passes per layer in the outlining strategies was kept the same, 500 passes for each layer. The respective paths of the precession beam when machining different diameters are illustrated in Figs. 5(a)–5(c). The relative offset positions of different layers from the top surface of the plates are also provided in Fig. 5. Specifically, the offset of the first layer or FPB in the outlining strategies was at 500 μm above the samples, and thus, FIB was close to the plate top surface. In this way, there was an efficient laser ablation at the first layer and, thus, the production of microholes with clean openings.

2. Full factorial experimental design

The three independent parameters investigated in this study were the incident angle, the FPB-FIB distance, and the scanning speed. A full factorial experimental design was used to analyze the effects of these key precession processing parameters and their interactions on the taper angle of the drilled holes together with their respective quality. The parameter ranges and their levels were narrowed down based on some initial drilling trials that produced successfully holes with acceptable quality. Specifically, the maximum range of incident angles available on the LS4 workstation, i.e., from 2.86° to 3.56°, was used. At the same time, the FPB-FIB distance in the range from 400 and 600 μm and scanning speeds up to 40 mm/s were identified as an effective processing domain for precession drilling of the holes. A further increase in the FPB-FIB distance led to a significant power drop of the output beam. The parameter domain considered in this study is provided in Table I. In addition, for a reference, holes were produced by conventional laser micromachining, i.e., helical drilling, to compare and quantify the advantages of precession laser processing. In conventional laser drilling, the laser beam was kept normal to the plate surface with the use of a telecentric focusing lens, and the beam was moved with the scanning head, only. A strategy with a hatch distance of 5 μm was deployed to remove all of the materials inside the holes. Scanning speed was set to be 1000 mm/s and pulse

TABLE I. Precession drilling parameters together with their respective three levels as used in full factorial experiments.

Factors	Unit	Value Level 1	Level 2	Level 3
Incident angle	Degree	2.86	3.22	3.56
FPB-FIB distance	μm	400	500	600
Speed	mm/s	10	25	40
No. of experiments with a precession beam		243		
No. of experiments with a conventional beam		9		
Total No. of experiments		252		

frequency of 100 kHz. A similar layer arrangement and pulse energy to precession machining was used in conventional laser machining. Each layer was repeated 100 times before the laser was refocused to the next layer.

D. Measurement and data analysis

The important output results from the conducted study were the taper angles of the produced microholes. The angles were calculated based on the difference between entrance and exit diameters of the drilled holes. The measurements of the hole entrances and exits were conducted on an Alicona G5 system with ×20 magnification. Scanning electron microscopy (SEM) images of the holes were taken, too, by using a JCM6000 system. Finally, x-ray computed tomography was used to analyze the machined sample with 5.1 μm

TABLE II. Taper angles attained in the experiments.

Order	Incident angle (degree)	FPB-FIB (μm)	Speed (mm/s)	Nickel alloy C265 substrate thickness (mm) 0.6 Hole diameter (μm) 100	250	500	1 Hole diameter (μm) 100	250	500	2 Hole diameter (μm) 100	250	500
1	2.86	400	10	1.30	1.47	0.95	0.55	0.54	0.21	1.61	1.46	1.66
2	2.86	400	25	1.79	1.68	1.55	0.56	0.69	0.73	1.72	1.76	2.27
3	2.86	400	40	2.22	2.23	3.57	0.72	0.77	1.65	1.95	2.05	2.97
4	2.86	500	10	0.91	0.83	0.36	0.31	0.31	0.00	1.75	1.53	1.58
5	2.86	500	25	1.55	1.42	1.11	0.29	0.34	1.14	1.88	1.86	2.21
6	2.86	500	40	1.77	2.06	3.74	0.61	0.44	1.55	1.99	2.31	2.83
7	2.86	600	10	0.81	0.89	0.08	0.13	0.48	0.02	1.98	1.59	1.40
8	2.86	600	25	1.11	0.88	1.06	0.24	0.43	1.96	2.02	1.87	1.85
9	2.86	600	40	1.47	1.11	4.31	0.46	0.44	1.85	2.14	2.28	2.35
10	3.22	400	10	1.12	1.43	0.75	0.36	0.46	0.50	1.89	1.46	1.57
11	3.22	400	25	1.50	1.92	1.23	0.57	0.58	0.75	1.88	1.66	1.80
12	3.22	400	40	1.92	2.45	3.80	0.70	0.65	2.01	2.05	1.94	2.46
13	3.22	500	10	0.83	1.33	0.27	0.23	0.31	0.12	1.98	1.34	1.48
14	3.22	500	25	1.22	1.59	1.12	0.20	0.34	1.01	2.18	1.55	1.75
15	3.22	500	40	1.55	2.02	4.04	0.41	0.42	2.26	2.25	1.94	2.38
16	3.22	600	10	0.87	0.85	−0.06	0.01	0.06	−0.03	1.87	1.24	1.28
17	3.22	600	25	0.97	0.99	0.93	0.10	0.22	1.08	2.15	1.43	1.54
18	3.22	600	40	1.18	1.59	4.31	0.45	0.19	2.40	2.29	1.74	2.28
19	3.56	400	10	1.68	1.20	0.60	0.42	0.69	0.30	1.90	1.22	1.59
20	3.56	400	25	1.54	1.31	0.90	0.55	0.77	1.62	2.14	1.58	1.88
21	3.56	400	40	2.05	1.90	3.35	0.66	0.88	2.21	2.25	1.92	2.45
22	3.56	500	10	1.14	0.93	−0.20	0.22	0.13	0.26	1.78	1.28	1.56
23	3.56	500	25	1.12	0.65	0.87	0.27	0.30	1.48	2.08	1.66	1.70
24	3.56	500	40	1.64	1.54	3.94	0.32	0.40	2.59	2.27	1.82	2.33
25	3.56	600	10	0.94	0.41	−0.13	0.00	0.16	−0.07	1.96	1.11	1.23
26	3.56	600	25	1.11	0.59	0.79	0.14	0.22	0.55	2.20	1.54	1.58
27	3.56	600	40	1.39	1.07	3.36	0.24	0.42	2.68	2.35	1.76	2.20
Conventional laser drilling	2.51	2.34	2.81	2.50	2.93	3.29	2.41	2.77	3.22			

resolution, 100 kV voltage, and 10 μA current. The experimental results were analyzed with Minitab statistics software to determine the effects of considered three process variables together with their interacts on taper angles of produced holes.

III. RESULTS AND DISCUSSION

A. Effects of key parameters

Taper angles obtained on the drilled holes are reported in Table II together with taper angles attained with the reference process, i.e., employing conventional laser micromachining. The smallest taper angles obtained for each hole diameter and substrate thickness are highlighted in gray. Note that the smallest taper angle in this research is the one closest to zero and not the one that has the absolute smallest value.

It is clear from the obtained results that the investigated key parameters, i.e., substrate thicknesses and hole diameters, had different effects. Figure 6 presents how the taper angle responded to these parameter variations. Pareto charts were also used to quantify the relative importance of these key parameters and their interaction effects on resulting taper angles based on their standardized effects (see Fig. 6). The reference line to analyze the factors' effects was drawn using Lenth's method in Minitab with a significance level of 0.05.[36]

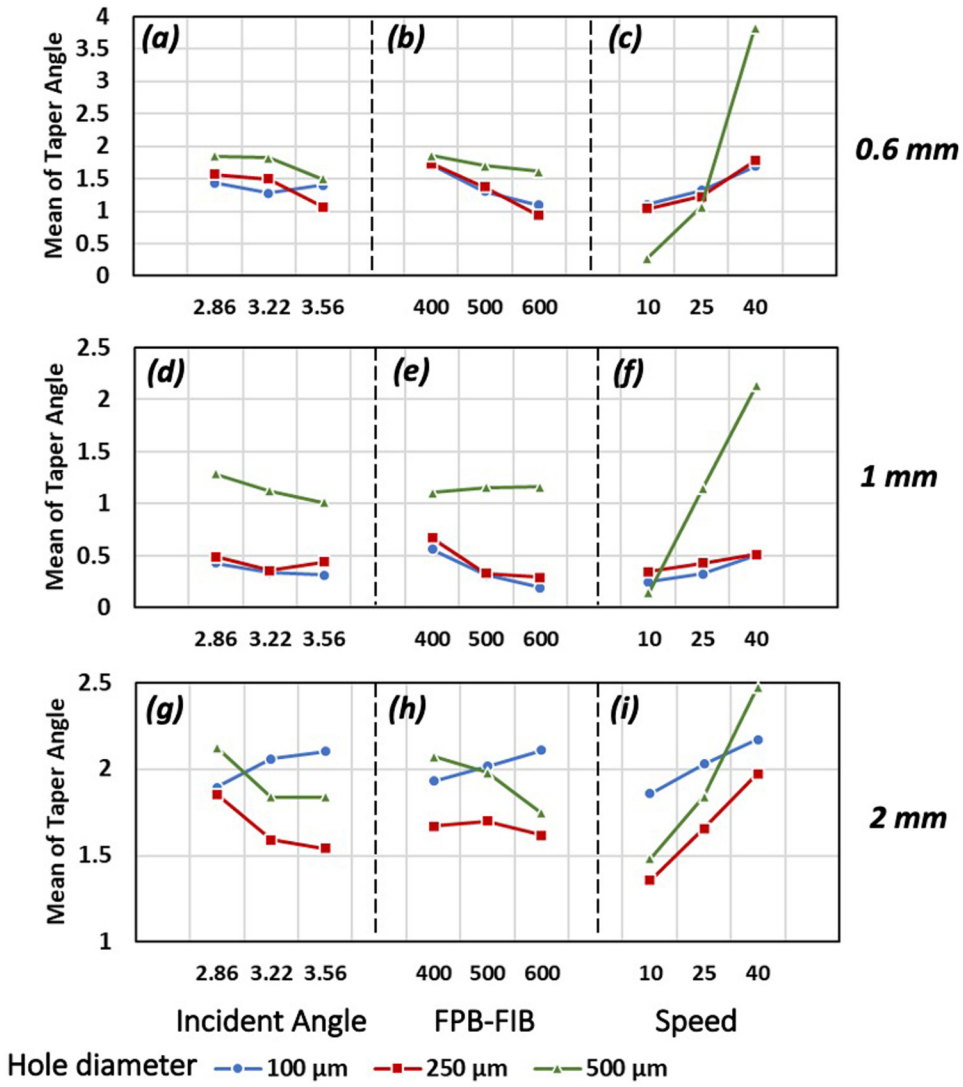

FIG. 6. Mean values of taper angles in regard to the parameter changes in precession drilling holes with diameters ranging from 100 to 500 μm on three substrate thicknesses: (a)–(c) 0.6 mm thickness, (d)–(f) 1 mm thickness, and (g)–(h) 2 mm thickness.

1. Effects of incident angle

Figures 6(a), 6(d), and 6(g) depict the effects of the incident angle on the taper angle of microholes drilled into 0.6, 1, and 2 mm substrates, respectively. It can be seen that the increase in incident angle led to a small/marginal decrease in taper angle in most of the cases. A bigger incident angle led to a bigger attacking angle in regard to the hole axis and side wall, too. Consequently, the laser beam spot area is reduced while fluence increases, which resulted in a more efficient ablation and a smaller taper angles can be achieved along the hole's side walls.[37] However, this is not the case for 100 μm hole drilled onto the 2 mm substrate, where the holes' aspect ratio was 20:1, and the increase in the incident angle led to a higher average taper angle. In this case, the precession beam was partially clipping the hole's entrance when the larger incident angle was applied, especially, when FPB was moved downward with a small entrance of just 100 μm. Specifically, it can be seen in Fig. 3 that the precession beam diameter was larger than 100 μm at more than 500 μm offset from the FPB position. This led to clipping of the precession beam at 100 μm entrance when FPB was more than 500 μm below the substrate top surface. In the case of 250 μm hole onto 1 and 2 mm thickness and 500 μm hole onto 2 mm thickness, the response of the taper angle mean value stabilized at the medium incident angle of 3.22°; thus, any further increases led to only marginal improvements. Nevertheless, the incident angle was found to be a statistically significant factor for all hole diameters except for 500 μm holes drilled into the 1 mm substrate [see Fig. 7(f)], where only scanning speed had a significant influence. However, the significance of the incident angle was much less than that of scanning speed and the FPB-FIB distance.

2. Effects of FPB-FIP distance

The effects of the FPB-FIB distance on the taper angle are presented in Figs. 6(b), 6(e), and 6(h). Specifically, the mean value of resulting taper angles decreased with the increase in the FPB-FIB distance and reached a minimum value at the FPB-FIB distance of 600 μm for most of the investigated diameters and substrate thicknesses. Positioning FPB at 500 μm above the substrate surface for the first layer led to FIB position of 100, 0, and −100 μm, respectively, when the FPB-FIB distance was varied from 400 to 600 μm. The ablation efficiency declined with the increase in hole aspect

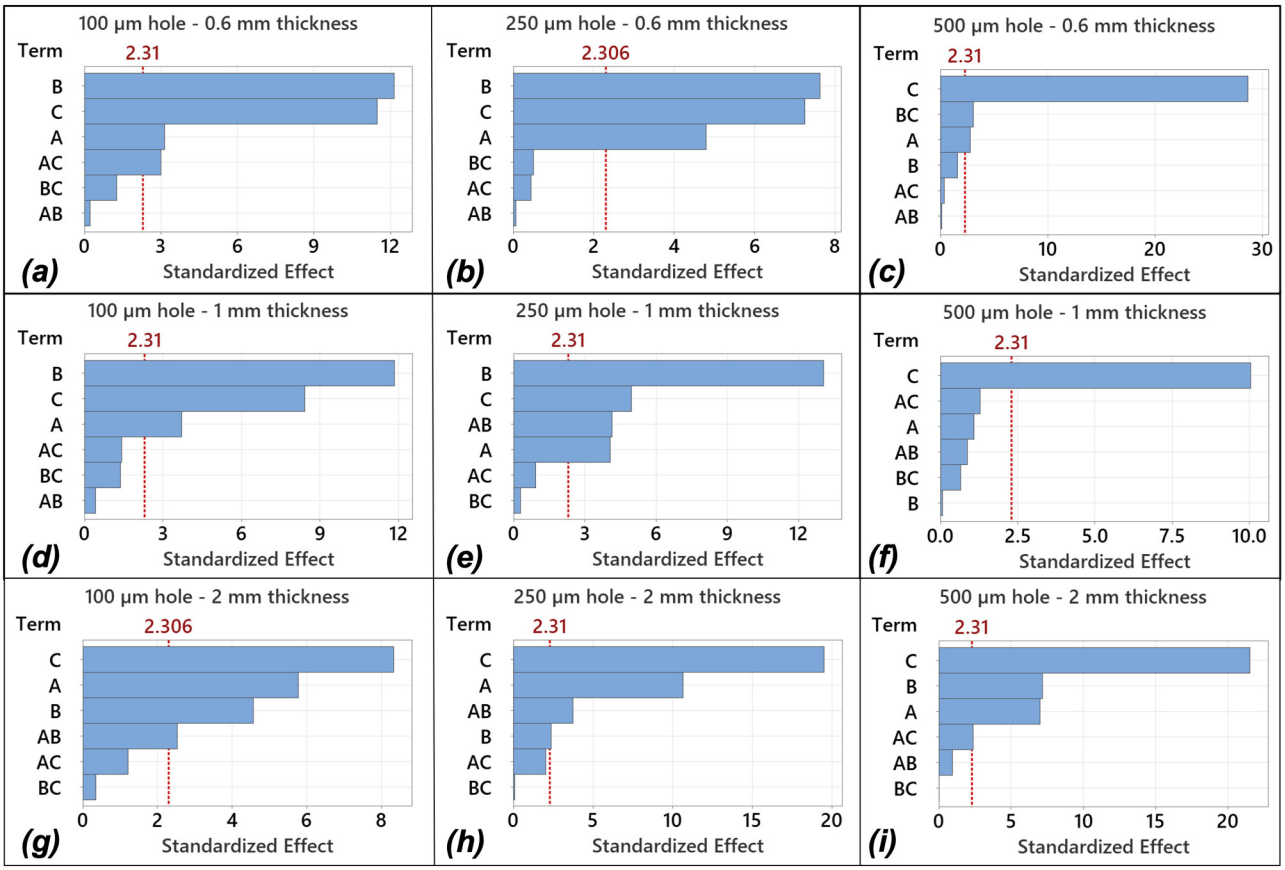

FIG. 7. Pareto charts on the significance of the investigated three factors, i.e., incident angle (a), the FPB-FIB distance (b), and scanning speed (c) when drilling holes onto: (a)–(c) 0.6 mm substrate, (d)–(f) 1 mm substrate, and (g)–(i) 2 mm substrate.

ratios as can be expected, and this could be attributed also to the processing with an offset from FIB. This was more pronounced when FIB was positioned at 100 μm, i.e., FPB-FIB distance of 400 μm. Focusing the beam below the substrate surface (−100 μm) improved the ablation response and material removal when the hole depths increased, especially when there was no beam refocusing (machining of 0.6 mm substrates). Thus, it can be stated that some beneficial effects on the taper angle was achieved indirectly.

Furthermore, the relationship between the taper angle and the FPB-FIB distance was close to linear compared to the effects of the incident angle. In contrast, 100 μm holes drilled on the 2 mm substrate showed an opposite effect on the taper angle, especially the larger FPB-FIB distance led to a higher tapering effect [Fig. 6(h)]. At the same time, the mean value of the taper angle was almost unaffected by the FPB-FIB distance when drilling 500 μm holes onto 1 mm substrates [Figs. 6(e) and 7(f)].

The Pareto chart [Figs. 7(a), 7(b), 7(d), and 7(e)] showed that the FPB-FIB distance was the most important factor when drilling 100 and 250 μm holes onto 0.6 and 1 mm substrates. The interaction effect of the incident angle and the FPB-FIB distance (AB) was also significant in drilling 100 μm holes onto 2 mm substrates and 250 μm holes onto 1 and 2 mm substrates [Figs. 7(e), 7(g), and 7(h)].

Figure 8 shows the x-ray cross-sectional views of drilled holes onto the substrates with different thicknesses. It is operant that the precession machining with an USP laser produces holes with almost no evidence of any abnormal material redeposition inside the holes. The obtained side walls were straight and consistent across the holes drilled onto 0.6 and 1 mm substrates, and thus, a better geometrical accuracy was achieved compared with the conventional drilling process. The holes drilled onto 2 mm substrates exhibited a sudden reduction in the holes' diameter near their exits [Figs. 8(g), 8(h), and 8(i)]. This is due to the reduced ablation efficiency with the depth increase and, hence, the increase in the aspect ratio. Although the beam was translated down into the material to assist the material removal, this also led to a partial clipping of the laser beam as discussed in Sec. III A 1. However, precession drilling still led to clear improvements when compared with results obtained with conventional laser drilling [Figs. 8(j) and 8(k)]. In addition, the FPB-FIB distance did not affect the entrance diameter of the hole.

3. Effects of scanning speed

The effects of scanning speed on the taper angle were the most pronounced among the investigated three factors. Consistent trends were observed for three hole diameters and substrate thicknesses used in the research. Figures 6(c), 6(f), and 6(i) show that the increase in scanning speed led to higher mean values of taper angle in all cases. This effect on the taper angle was opposite to the general trend attained when increasing both the incident angle and the FPB-FIP distance. This can be attributed to the interdependence between accumulated fluence and scanning speed. Specifically, a higher speed at a constant repetition rate (100 kHz) resulted in lower pulse overlap level and less accumulated pulse energy when the same scanning strategies were executed. It is worth noting that the effect of scanning speed on the taper angle

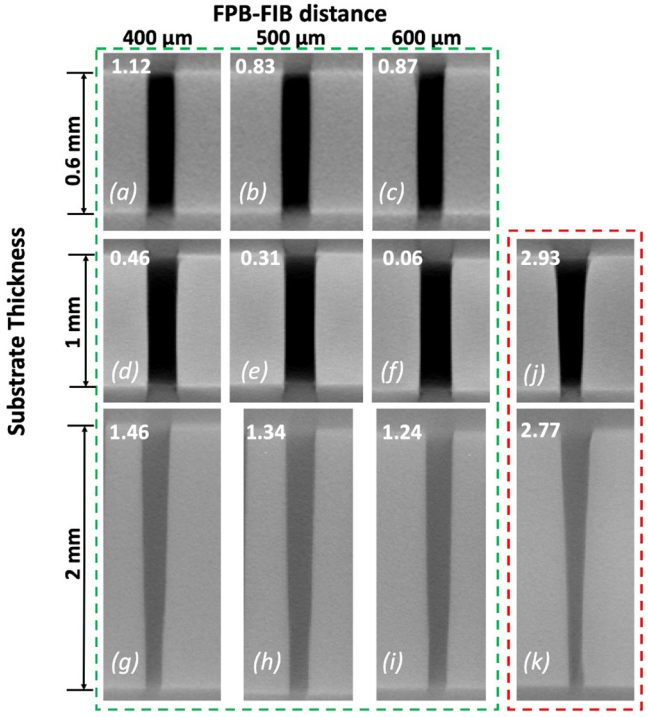

FIG. 8. X-ray cross-sectional views of holes produced by precession (green dashed line) and conventional (red dashed line) drilling onto substrates with three thicknesses and varying FPB-FIB distances: (a)–(c): 100 μm holes onto the 0.6 mm substrate; (d)–(f) 250 μm holes on the 1 mm substrate; (g)–(i) 250 μm holes on the 2 mm substrate; (j) and (k): 250 μm holes on 1 and 2 mm substrates, respectively. All holes were drilled with an incident angle of 3.22° and a scanning speed of 10 mm/s. Corresponding taper angle of each hole is showed in the top left corner of each image.

was the most linear one among the investigated three precession drilling parameters.

Furthermore, the effect of scanning speed was much more pronounced in the case of 500 μm holes across all three substrate thicknesses. Figures 5(a)–5(c) show that the beam paths in the case of 100 and 250 μm hole diameters were much closer to each other compared to the 500 μm hole. In fact, the employed beam paths

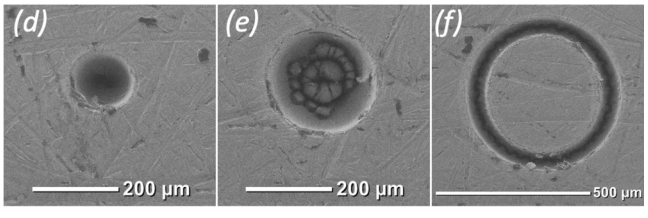

FIG. 9. Hole's opening produced by employed strategies for different diameters: (a) 100, (b) 250, and (c) 500 μm.

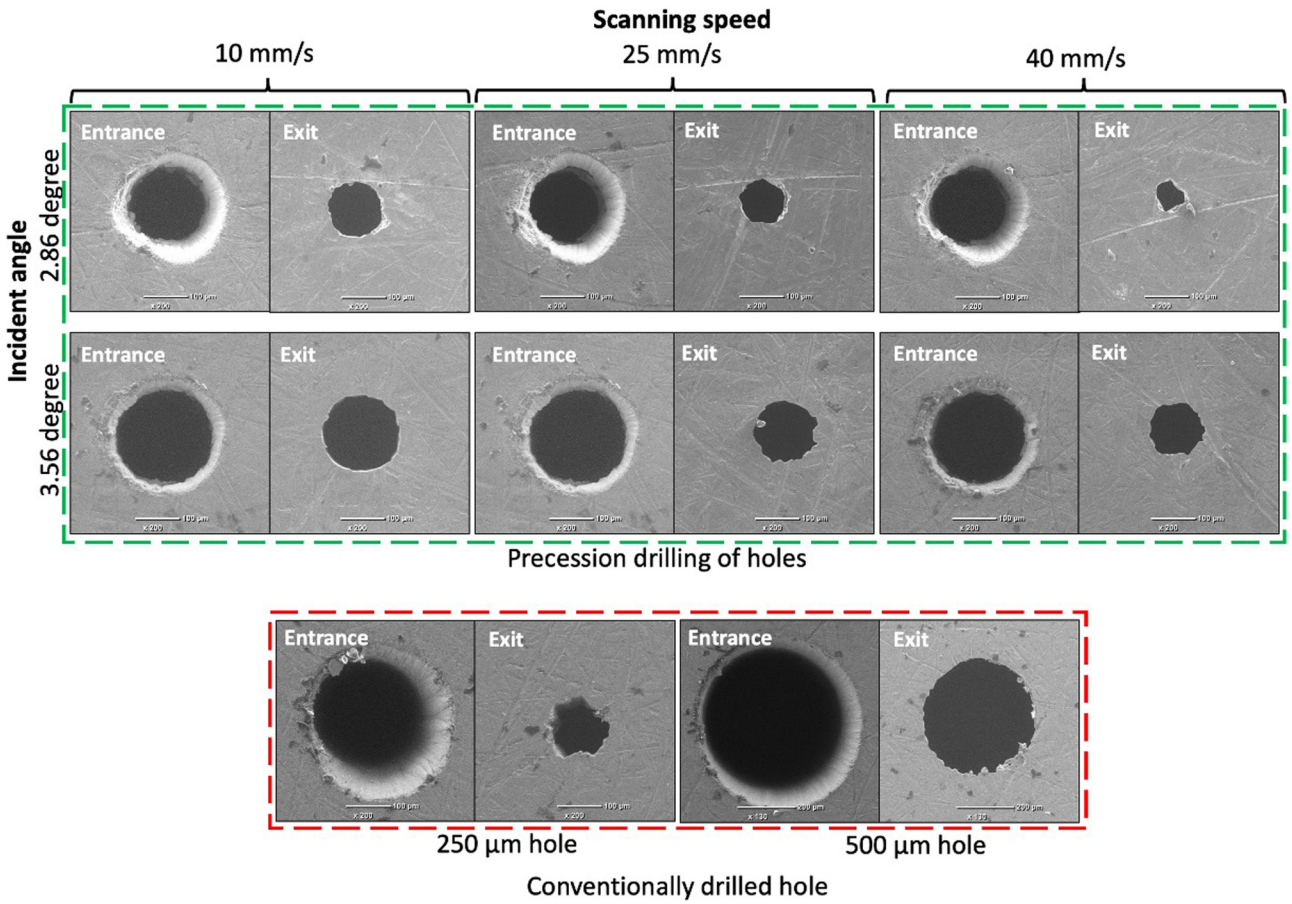

FIG. 10. Entrances and exits of 250 μm holes produced by precession drilling while a FPB-FIB distance fixed at 600 μm and different scanning speeds and incident angles on the 2 mm substrate (green dashed line). Entrances and exits of 250 and 500 μm holes drilled onto the 2 mm substrate with the conventional laser drilling process (red dashed line).

covered almost entirely the hole's area (100% of hole's area) and all materials inside the holes were removed in the case of 100 and 250 μm holes [Figs. 9(a) and 9(b)]. At the same time, the beam paths covered much smaller percentage of hole's area (39% of hole's area) and removed only the outer material of 500 μm holes and left a "core" inside [Fig. 9(c)]. In addition, the beam passes in the layers for the smaller diameter holes required a shorter scanning time. As a result, this led to some heat accumulation and its impact on the ablation process was less affected by the varying scanning speed when machining smaller holes. Contrarily, the larger holes required a longer time for each beam pass in the layers, and thus, there was more time for heat conduction into the material to take place. Consequently, the effect of scanning speed on ablation efficiency was much higher and, therefore, led to a significant increase in the taper angle. Specifically, the steep increase in the taper angle from approximately 0.25° to 3.8° with the increase in the scanning speed from 10 to 40 mm/s, respectively, on a 0.6 mm substrate [see Fig. 6(c)] is another strong evidence of the

TABLE III. Optimum values of investigated precession drilling parameters for producing microholes with a minimum taper angle onto C263 substrates with three different thicknesses.

Thickness (mm)	Target hole diameter (μm)	Optimum key parameters: Incident angle (degree)	FPB-FIB (μm)	Speed (mm/s)	Obtained taper angle
0.6	100	2.86	600	10	0.81
	250	3.56	600	10	0.41
	500	3.22	600	10	−0.06
1	100	3.56	600	10	0.00
	250	3.22	600	10	0.06
	500	3.56	600	10	−0.07
2	100	2.86	400	10	1.61
	250	3.56	600	10	1.11
	500	3.56	600	10	1.23

heat conduction impact on the ablation process and consequently on the taper angle.

Scanning speed was one of the most significant factors in five cases [Figs. 7(c), 7(f), and 7(g)–7(i)] and was always into the top two most important factors across the three hole diameters and substrate thicknesses. In addition, it can be seen from Figs. 6 and 7 that the impact of speed on 100 and 250 μm diameter were quite similar for all three substrate thicknesses. At the same time, the influence of scanning speed strongly dominated the effects of other two factors in drilling 500 μm holes. Specifically , scanning speed was the only factor that had a significant impact on the tapering effect when drilling 500 μm hole onto 1 mm substrates [Fig. 7(f)]. In addition, the interaction effect of scanning speed and incident angle (AC) was found to be significant only in drilling 100 μm hole onto the 0.6 mm substrate.

Some examples depicting the effects of scanning speed and incident angle on holes' entrances and exits are presented in Fig. 10. Scanning speed did not have a noticeable effect on hole entrances. The scanning speeds investigated in this research were sufficient to achieve the accumulated fluence necessary for producing holes with clean entrances, even at highest scanning speed of 40 mm/s. However, a clear reduction in exit diameters can be seen when the speed increased from 10 to 40 mm/s regardless of incident angles. At the same time, the effect of the incident angle on the taper angle was confirmed, i.e., when the increase in the incident angle led to larger exit diameters (see Fig. 10), while the hole entrances were also affected. Specifically, the incident angle of 3.56° led to a better edge definition and slightly bigger entrance than the incident angle of 2.86°. In general, the dimensional accuracy and circularity of holes produced by precession drilling were better than those produced with the conventional laser drilling process.

B. Process optimization

The optimal parameters for precession drilling holes with a minimized taper angle onto the C263 substrates with three different thicknesses are provided in Table III. The minimum taper angles for all three hole diameters and substrate thicknesses were achieved at a scanning speed of 10 mm/s. This underlines the importance of speed, i.e., the pulse overlap levels in precession laser machining, on improving the ablation efficiency due to higher heat accumulation at the low speed. The higher FPB-FIB distances of 600 μm were also important for attaining a minimum taper angle. At the same time, higher incident angles are beneficial in precession drilling bigger holes, while the machining of smaller ones requires a carefully consideration of the trade-offs between the incident angle and the interaction effects between other parameters. Figure 11 shows the entrances and exits of the holes machined with optimal precession parameters. The impact of the substrate thickness is very well pronounced in the case of 100 μm holes, where the exit diameter decreased significantly with the thickness increase from 1

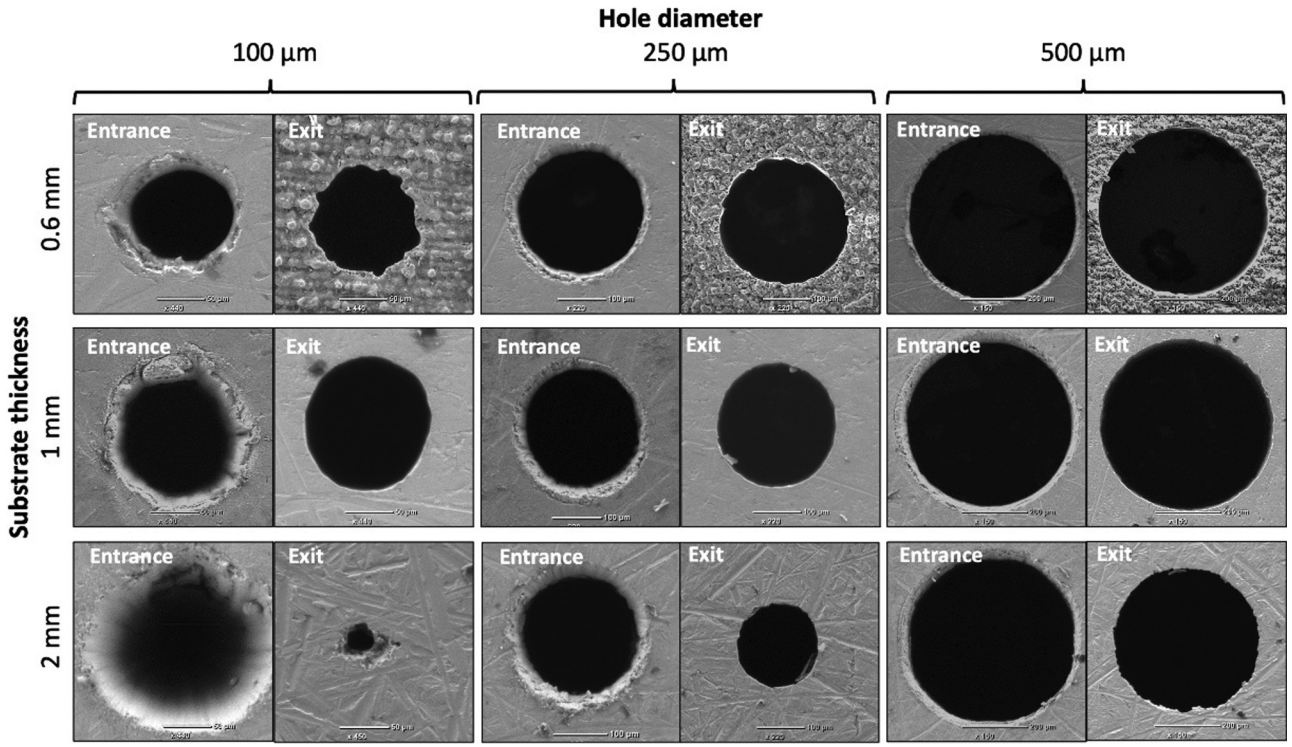

FIG. 11. Holes' entrances and exits when the minimum taper angles were achieved by the precession drilling process on three investigated substrate thicknesses.

to 2 mm, and the precession drilling process managed to penetrate only barely the 2 mm substrate. Thus, the high aspect ratios in drilling thicker substrates are still a challenge even when precession laser machining is employed. Based on the conducted empirical study, the substrate thickness of 1 mm can be considered the upper limit for achieving a zero-taper angle with the precession drilling process.

IV. CONCLUSION

The results reported in this study provides an insight into capabilities and limitations of precession laser machining, both in general about the effects of key precession processing parameters on dimensional and geometrical accuracy of microholes and also about one specific application, i.e., drilling of nickel alloy C263. The precession drilling of holes with diameters from 100 to 500 μm onto substrates with thicknesses up to 2 mm, aspect ratios up to 20:1, was investigated. The effects of three key parameters, i.e., incident angle, FPB-FIB distance, and scanning speed, in precession laser drilling were analyzed. The taper angle of the microholes was used as a key output quality factor to determine the effects of the investigated three parameters. The results showed that all three parameters affected the precession drilling process but to different extends.

Generally, the increase in the incident angle and the FPB-FIB distance led to a taper angle reduction in most of the cases. In contrast, the increase in the scanning speed entailed a taper angle increase. However, the precession drilling process was affected by a beam clipping at the hole entrance when machining high aspect ratio hole or thicker substrates. This beam clipping affected the ablation efficiency with the increase in the hole depth and led to a taper angle increase. Nonetheless, it was possible to precession drill holes with nearly zero or even a negative taper angle onto 0.6 and 1 mm substrates, which was impossible to achieve employing the conventional laser drilling process. Also, a significant reduction in holes' taper angle was achieved on 2 mm substrates, where the aspect ratios were up to 20:1, compared with conventional laser drilling.

In summary, the precession drilling process has demonstrated clear advantages in producing microholes with a higher dimensional and geometrical accuracy when optimized processing strategies were applied. Moreover, the precession machining setups can be developed further to avoid any beam clipping and consequent power dropping and, thus, to use fully the attractive processing capabilities offered by this machining method.

ACKNOWLEDGMENTS

The authors would like to acknowledge the support obtained through the UKRI Future Leaders Fellowship under Grant No. MR/V02180X/1 and the collaboration with LASEA SA, Belgium within the framework of the ESIF project "Smart Factory Hub" (SmartFub).

AUTHOR DECLARATIONS

Conflict of Interest

The authors have no conflicts to disclose.

Author Contributions

Hoang Le: Conceptualization (lead); Data curation (lead); Formal analysis (lead); Investigation (lead); Methodology (lead); Software (lead); Visualization (lead); Writing – original draft (lead); Writing – review & editing (lead). **Vahid Nasrollahi:** Formal analysis (supporting); Methodology (supporting); Writing – review & editing (supporting). **Themistoklis Karkantonis:** Conceptualization (supporting); Writing – review & editing (supporting). **Pavel Penchev:** Methodology (supporting); Writing – review & editing (supporting). **Sundar Marimuthu:** Writing – review & editing (supporting). **Mickey Crozier:** Resources (supporting). **Stefan Dimov:** Conceptualization (supporting); Funding acquisition (lead); Methodology (supporting); Supervision (lead); Writing – review & editing (supporting).

REFERENCES

[1]S. Pattanayak and S. Panda, "Laser beam micro drilling—A review," Lasers Manuf. Mater. Process. **5**, 366–394 (2018).
[2]R. A. Krüger, M. Schulz-Ruhtenberg, B. Rösener, O. Ostermann, R. Ostholt, and N. Ambrosius, "LIDE high aspect ratio glass processing technology for the mass production of microfluidic devices for biomedical applications," in *Microfluidics, BioMEMS, and Medical Microsystems XVII* (SPIE, Bellingham, WA, 2019).
[3]H.-J. Wang and T. Yang, "A review on laser drilling and cutting of silicon," J. Eur. Ceram. Soc. **41**, 4997–5015 (2021).
[4]M. Sharp, "Laser processing of medical devices," in *Biophotonics for Medical Applications* (Woodhead, Cambridge, 2015), pp. 79–98.
[5]S. Marimuthu, M. Antar, and J. Dunleavey, "Characteristics of micro-hole formation during fibre laser drilling of aerospace superalloy," Precis. Eng. **55**, 339–348 (2019).
[6]G. D. Gautam and A. K. Pandey, "Pulsed Nd YAG laser beam drilling A review," Opt. Laser Technol. **100**, 183–215 (2018).
[7]X. Jia, Y. Zhang, Y. Chen, H. Wang, G. Zhu, and X. Zhu, "Combined pulsed laser drilling of metal by continuous wave laser and nanosecond pulse train," Int. J. Adv. Manuf. Technol. **104**, 1269–1274 (2019).
[8]P. Petkov, S. S. Dimov, R. M. Minev, and D. T. Pham, "Laser milling: Pulse duration effects on surface integrity," Proc. Inst. Mech. Eng. Part B: J. Eng. Manuf. **222**, 35–45 (2008).
[9]A. Weck, T. H. R. Crawford, D. S. Wilkinson, H. K. Haugen, and J. S. Preston, "Laser drilling of high aspect ratio holes in copper with femtosecond, picosecond and nanosecond pulses," Appl. Phys. A **90**, 537–543 (2008).
[10]A. H. Hamad, "Effects of different laser pulse regimes (nanosecond, picosecond and femtosecond) on the ablation of materials for production of nanoparticles in liquid solution," in *High Energy and Short Pulse Lasers* (IntechOpen, London, 2016).
[11]H. Duc Doan, I. Naoki, and F. Kazuyoshi, "Laser processing by using fluidic laser beam shaper," Int. J. Heat Mass Transfer **64**, 263–268 (2013).
[12]H. Le, P. Penchev, A. Henrottin, D. Bruneel, V. Nasrollahi, J. A. Ramos-de-Campos, and S. Dimov, "Effects of top-hat laser beam processing and scanning strategies in laser micro-structuring," Micromachines **11**, 221 (2020).
[13]V. Nasrollahi, P. Penchev, T. Jwad, S. Dimov, K. Kim, and C. Im, "Drilling of micron-scale high aspect ratio holes with ultra-short pulsed lasers: Critical effects of focusing lenses and fluence on the resulting holes' morphology," Opt. Lasers Eng. **110**, 315–322 (2018).
[14]B. Bhattacharyya and B. Doloi, "Chapter Four—Machining processes utilizing thermal energy," in *Modern Machining Technology*, edited by B. Bhattacharyya and B. Doloi (Academic, London, 2020), pp. 161–363.
[15]M. Hasan, J. Zhao, and Z. Jiang, "A review of modern advancements in micro drilling techniques," J. Manuf. Process. **29**, 343–375 (2017).

[16]S. H. Kim, T. Balasubramani, I. B. Sohn, Y. C. Noh, J. Lee, J. B. Lee, and S. Jeong, "Precision microfabrication of AlN and Al_2O_3 ceramics by femtosecond laser ablation," in *Photon Processing in Microelectronics and Photonics VII, 21–24 January 2008, San Jose, CA* (SPIE, Bellingham, WA, 2008).
[17]L. Calabrese, M. Azzolini, F. Bassi, E. Gallus, S. Bocchi, G. Maccarini, G. Pellegrini, and C. Ravasio, "Micro-milling process of metals: A comparison between femtosecond laser and EDM techniques," J. Manuf. Mater. Process. **5**, 125 (2021).
[18]V. Tangwarodomnukun and C. Dumkum, "Experiment and analytical model of laser milling process in soluble oil," Int. J. Adv. Manuf. Technol. **96**, 607–621 (2018).
[19]V. Nasrollahi, P. Penchev, A. Batal, H. Le, S. Dimov, and K. Kim, "Laser drilling with a top-hat beam of micro-scale high aspect ratio holes in silicon nitride," J. Mater. Process. Technol. **281**, 116636 (2020).
[20]A. Salama, Y. Yan, L. Li, P. Mativenga, D. Whitehead, and A. Sabli, "Understanding the self-limiting effect in picosecond laser single and multiple parallel pass drilling/machining of CFRP composite and mild steel," Mater. Des. **107**, 461–469 (2016).
[21]P.-E. Martin, S. Estival, M. Dijoux, A. Kupisiewicz, and R. Braunschweig, "Laser cutting and drilling with zero conicity," J. Laser Appl. **29**, 022211 (2017).
[22]See https://www.lasea.eu/en/oem/ls-precess/ for "LASEA.: LS-Precess," (2021) [cited 22 June 2022].
[23]See https://uk.aerotech.com/product/laser-scan-heads-en-uk/agv5d-five-axis-laser-micromachining-precession-scanner/ for "Aerotech.: AGV5D five-axis laser micromachining precession scanner," (2022) [cited 22 June 2022].
[24]N. Photonics, see https://novantaphotonics.com/product/precession-elephant-2/ for "Precession Elephant 2," (2022) [cited 22 June 2022].
[25]See https://www.scanlab.de/en/products/advanced-scanning-solutions/precsys-micromachining-system for "Scanlab.: precSYS micromachining system," (2022) [cited 22 June 2022].
[26]J. Auerswald, A. Ruckli, T. Gschwilm, P. Weber, D. Diego-Vallejo, and H. Schlüter, "Taper angle correction in cutting of complex micro-mechanical contours with ultra-short pulse laser," J. Mech. Eng. Autom. **6**, 334–338 (2016).
[27]T. L. See, Z. Liu, H. Liu, L. Li, J. Chippendale, S. Cheetham, and S. Dilworth, "Effect of geometry measurements on characteristics of femtosecond laser ablation of HR4 nickel alloy," Opt. Lasers Eng. **64**, 71–78 (2015).
[28]W. Zhao, H. Liu, X. Shen, L. Wang, and X. Mei, "Percussion drilling hole in Cu, Al, Ti and Ni alloys using ultra-short pulsed laser ablation," Materials **13**, 31 (2019).
[29]N. Semaltianos, W. Perrie, P. French, M. Sharp, G. Dearden, S. Logothetidis, K. G. Watkins, "Femtosecond laser ablation characteristics of nickel-based superalloy C263," Appl. Phys. A **94**, 999–1009 (2009).
[30]H. Le, C. Pradhani, P. Penchev, V. Nasrollahi, T. Karkantonis, Y. Wang, S. Dimov, and J. A. Ramos-de-Campos, "Laser precession machining of cross-shaped terahertz bandpass filters," Opt. Lasers Eng. **149**, 106790 (2022).
[31]S. Estival, P.-E. Martin, and A. Kupisiewicz, "Machining device," U.S. patent US010279426B2 (2019).
[32]P.-E. Martin, S. Estival, M. Dijoux, A. Kupisiewicz, and R. Braunschweig, "Laser cutting and drilling with zero conicity," in *Laser-based Micro-and Nanoprocessing XI, San Francisco, CA* (SPIE, Bellingham, WA, 2017).
[33]P. Mastanaiah, G. Madhusudhan Reddy, K. Satya Prasad, and C. V. S. Murthy, "An investigation on microstructures and mechanical properties of explosive cladded C103 niobium alloy over C263 nimonic alloy," J. Mater. Process. Technol. **214**, 2316–2324 (2014).
[34]S. J. Davies, S. P. Jeffs, M. P. Coleman, and R. J. Lancaster, "Effects of heat treatment on microstructure and creep properties of a laser powder bed fused nickel superalloy," Mater. Des. **159**, 39–46 (2018).
[35]R. K. Shastri and C. P. Mohanty, "Sustainable electrical discharge machining of Nimonic C263 superalloy," Arabian J. Sci. Eng. **46**, 7273–7293 (2021).
[36]R. Xampeny, P. Grima, and X. Tort-Martorell, "Selecting significant effects in factorial designs: Lenth's method versus using negligible interactions," Commun. Stat.-Simul. Comput. **47**, 1343–1352 (2018).
[37]A. Michalek, A. Batal, S. Qi, P. Penchev, D. Bruneel, T. L. See, and S. Dimov, "Modelling ultrafast laser structuring/texturing of freeform surfaces," Appl. Surf. Sci. Adv. **2**, 100036 (2020).